PHYSICAL REVIEW E **85**, 021309 (2012)

Onset of irreversibility in cyclic shear of granular packings

Steven Slotterback,[1,*] Mitch Mailman,[1] Krisztian Ronaszegi,[1] Martin van Hecke,[2] Michelle Girvan,[1] and Wolfgang Losert[1,†]
[1]*Department of Physics, and IREAP, University of Maryland, College Park, Maryland 20742, USA*
[2]*Kamerlingh Onnes Laboratory, Universiteit Leiden, P.O. Box 9504, NL-2300RA Leiden, The Netherlands*
(Received 23 September 2011; published 27 February 2012)

We investigate the onset of irreversibility in a dense granular medium subjected to cyclic shear in a split-bottom geometry. To probe the micro- and mesoscale, we image bead trajectories in three dimensions throughout a series of shear strain oscillations. Although beads lose and regain contact with neighbors during a cycle, the global topology of the contact network exhibits reversible properties for low oscillation amplitudes. With increasing reversal amplitude, a transition to an irreversible diffusive regime occurs.

DOI: 10.1103/PhysRevE.85.021309 PACS number(s): 45.70.−n, 47.57.Gc, 64.60.aq, 64.60.ah

I. INTRODUCTION

The transition from reversible to irreversible dynamics in systems of many interacting particles is of fundamental importance to many-body physics. Granular materials under repeated shear deformations constitute excellent experimental systems with which to study such reversibility for out-of-equilibrium systems. Since grains are macroscopic in size, thermal fluctuations are negligible [1], with particle trajectories determined by contact forces between neighboring grains. In groundbreaking work on low-concentration granular suspensions, Corté and coworkers observed that particle collisions tend to disrupt the inherent reversibility of low-Reynolds-number fluid flow and that reversibility is lost at strains and densities that allow a particle to collide with two or more neighbors [2]. As a consequence, the onset of irreversibility decreases approximately as the square of the particle density [3].

For dense particle systems close to jamming, the threshold for exact spatial reversibility would thus become extremely small. However, dense configurations of particles have additional constraints on their positions: the neighborhood of nearby grains in the local environment of the particle confines its position, providing a new reference for the motion of the particle. This perspective opens up the possibility of an alternative form of reversibility with respect to the local neighborhood of particles. Under shear strain, neighbors are lost, and correlations are important: rearrangements in dense configurations are highly collective and are known to exhibit a range of dynamical features, from local reversibility as found in foams [4] to larger scale dynamical heterogeneities as found in two-dimensional (2D) bidisperse cylinders [5–7].

In this article, we describe experiments that explore strains for which these rearrangements first emerge at scales larger than a grain diameter. Since we probe extremely slow strain rates, the granular temperature is virtually zero and rearrangements are due to plastic deformations as opposed to random motion. We characterize the local environment around particles and the plastic deformations, through the analysis of the network of nearby particles. In our experiments, the full 3D motion of beads within a split-bottom shear cell undergoes cyclic shear. Dense granular systems under cyclic shear in two and three dimensions have been studied previously [5,8–11], but the trajectories of all beads in the bulk have not been probed, and collective bead dynamics and reversibility are not well understood.

We find that mean square displacements (MSDs) of beads indicate a crossover between two behaviors and that a characteristic strain amplitude is associated with this crossover. In order to relate this change in behavior to changes in the neighbor network, we analyze neighbor changing events through the use of the broken link (BL) network [12], which assigns a link to pairs of particles that then later move apart, under shear strain. For strain amplitudes below the aforementioned characteristic amplitude, the largest interconnected component of the BL network nearly disappears after shear reversal, while above the characteristic amplitude a giant component appears to emerge and survive the shear reversal. We posit a novel type of reversibility/irreversibility transition under cyclic shear strain: one that distinguishes between a regime where rearrangements are essentially local and random, never leading to a qualitative change in the topology of the BL network, and a regime where the topology is modified significantly by the formation of a giant component. We refer to this phenomenon as "topological irreversibility," by virtue of the fact that the topology of the BL network is being irreversibly altered by the formation of a giant component.

II. EXPERIMENTAL PROCEDURE AND RESULTS

A. Setup

To study the motion of all beads, we built a modified version of the split-bottom geometry [13,14] that allows for 3D imaging. In this geometry, shear is applied from below by rotating a disk mounted flush with the bottom. A shear zone is then emanating from the edge of a rotating disk; much of the shear zone is far from boundaries, the shear zone is wide and smooth, and nothing obstructs its view, making it ideally suited for 3D observations of grain flows with smooth gradients.

We use a square box with a 15 × 15-cm bottom and a 9-cm-diameter disk at the bottom. In order to provide traction for the beads above, we attach a sparse coating of 3-mm beads to the bottom of the container and disk surface. We fill the container with 3/16-in.-diameter acrylic beads. We immerse the beads in an index-matched fluid (Triton X-100). A fluorescent dye

*scsumd@umd.edu
†wlosert@umd.edu

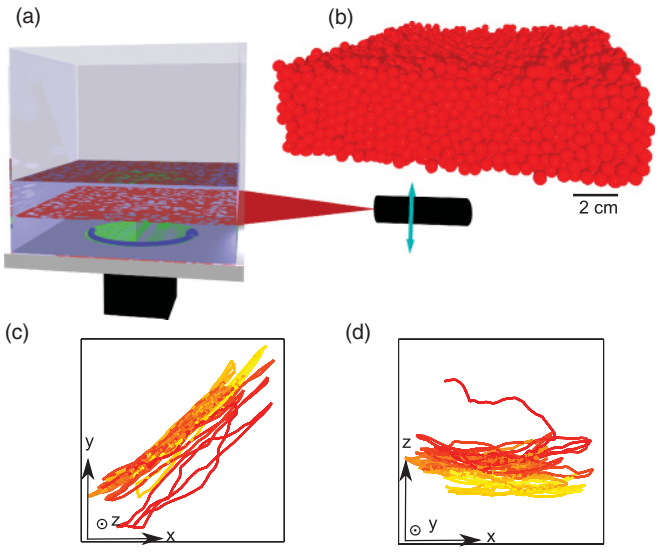

FIG. 1. (Color online) (a) Split-bottom shear cell with acrylic beads in index-matched, dyed fluid. A laser sheet illuminates cross sections for imaging. (b) As shown in this reconstruction, the position of all beads is found by scanning of the laser sheet across the whole container and automatic particle recognition. (c, d) Typical trajectory of a bead under oscillatory shear strain with a reversal amplitude of 40° from (c) above and (d) the side. Cube sides are 2 bead diameters; the color changes from dark gray (red) to light gray (yellow) with increasing time.

(Nile Blue 690 perchlorate) is added to the fluid, along with a small amount of HCl (1.0 ml/1.0 L of fluid) to stabilize the mixture.

We use the 3D imaging technique described in [15] and illustrated in Fig. 1, but with an improved bead finding algorithm. We use a 3D version of the convolution described in [16] to find the position of each bead to better than half a pixel, or 4% of a bead diameter. We then track the motion of individual beads with a tracking algorithm developed by Grier *et al.* [17] to find trajectories such as the one in Figs. 1(c) and 1(d). With the full trajectories for about 98% of beads in our system outside the bottom layer, we can now analyze how beads move with respect to their neighbors.

We choose to fill the container to a filling height H equal to the radius of the shearing disk R_s. This regime, which has only been approached experimentally in a limited number of studies [12,18,19], is between two predicted regimes wherein the shear bands in a constant strain angular velocity profile transition from annular regions that widen above the disk edge ($H/R_s < 0.7$) to a dome-shaped region above the disk ($H/R_s \gg 1$) [20]. We choose this intermediate regime in order to maximize the fraction of grains undergoing differential flow.

The angular velocity flow field is quite heterogeneous in the case of constant shear. The differential flow, as shown in [12], is greatest in a region above the shearing disk. We choose to limit our analysis to this region of maximum relative strain. We find this region by calculating the mean angular velocity in annular regions about the axis of disk rotation. We disregard axial and radial velocities, since the bulk remains stationary on average. We use these values to find the approximate differential strain in the axial and radial directions. The regions with relative strains in the lower 60th percentile are excluded.

Imaging cannot distinguish whether two hard spheres are in contact or just close together; instead, we choose a maximum separation criterion to identify the nearest neighbors of each bead based on a preference for tangential motion of neighboring beads [12,21]. Based on this criterion, we consider beads whose centers are within ≈1.08 bead diameter of one another to be nearest neighbors, since beads that are separated by greater distances show no such preference for tangential relative motion. Thus, the beads have an effective radius $R = 0.54$ bead diameter.

B. Protocol

To create reproducible initial conditions representative of steady shear, we rotate the disk two full revolutions at 1 mrad/s. At this rate of strain, the granular flow in our fluid immersed system is independent of the strain rate, with the same velocity profile as a dry granular flow [22]. We then reverse the direction of rotation of the disk and move the disk for a strain of θ_r (=2°,4°,10°,20°,40°). We reverse the direction again and rotate the disk by $-\theta_r$ to its original position, thus straining and reversing the system in a cyclic fashion. We perform 20 successive cycles in each experiment, taking a 3D image of the system after every 2° of strain.

C. Mean square displacements

The first measure of reversibility we employ is to test how far a bead has moved after a full cycle. The MSDs of the beads in the shear zone at the end of each of the 20 cycles are shown as function of cycle number, n_c, in Fig. 2(a). For all but the highest reversal amplitude θ_r, the slope of the MSD decreases with increasing cycle number to slopes below 1, signaling subdiffusive behavior.

To explore whether the system becomes more reversible after several shear cycles, we choose the beginning frame of a later starting cycle, n_s, as a reference frame. Figure 2(b) illustrates that for $n_s = 10$, the MSD is up to an order of magnitude smaller, suggesting that bead positions in this cyclic shear flow become more reversible after several cycles. Strikingly, the MSD for the highest reversal amplitude ($\theta_r = 40°$) is considerably larger in magnitude.

To compare the rearrangements after one cycle of amplitude θ_r with two cycles of amplitude $\theta_r/2$, etc., we calculate the MSD after a fixed absolute strain $\Delta\theta$ (relative to a chosen reference frame) which we fix here at 80°. Figure 2(c) shows the MSD at this fixed total strain as a function of the start cycle n_s. We see that for $\theta_r = 40°$, the magnitude of the MSD does not depend strongly on the choice of reference cycle after a short transient of about three cycles, while the MSDs for smaller θ_r continue a downward trend for all cycles investigated.

In terms of spatial reversibility, where all beads return to their original coordinates, all three probes of the MSD strongly suggest a qualitative change in behavior between $\theta_r = 20°$ and $\theta_r = 40°$: for a high amplitude, the motion is irreversible and reaches a steady, diffusive state, while for low amplitudes, the

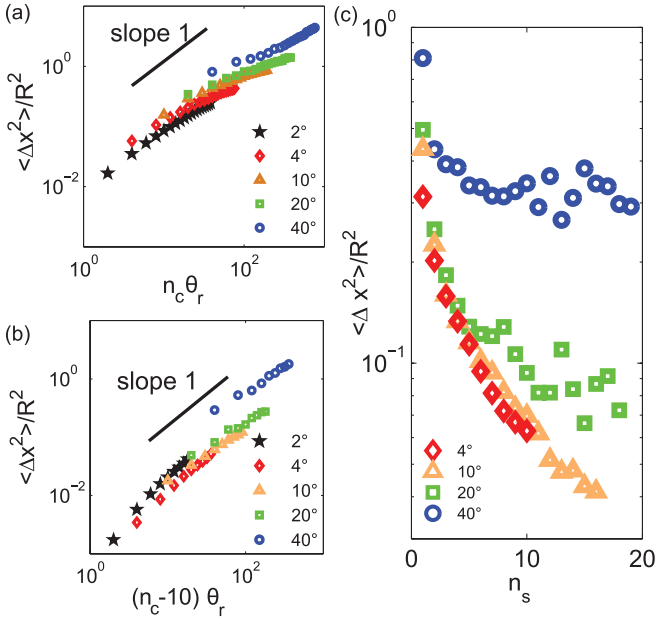

FIG. 2. (Color online) Mean square displacements (MSDs) at the end of each cycle as a function of cycle number for different cycle amplitudes, scaled by the effective bead radius R. (a) Reference frame at the start of the first cycle. (b) The start of the 10th cycle is chosen as a reference frame. (c) MSD after 80° of absolute strain vs reference cycle number.

cyclic shear strain process becomes increasingly reversible (i.e., decreasing MSD magnitudes) and the system is aging.

D. Broken links

As a second measure of reversibility we probe the network of nearest neighbors. We first identify all neighbors in a reference frame at the start of a cycle. Then we calculate, as a function of the frame number, the fraction of links broken f_b, defined as the fraction of neighbor pairs from the reference frame that are no longer within the cutoff distance used to define neighbors. The approach of [12] has been modified here to include the possibility of "healing." A link is healed when a neighbor pair from the reference frame that has been broken later re-forms. A healed link does not appear in the BL network. Note that other pairs of beads may become neighbors in later frames but this is not considered in the BL analysis.

In Fig. 3(a) we show the evolution of f_b as a function of $\Delta\theta$, for $\theta_r = 10°$; other θ_r values show comparable results. The top curve shows f_b with $n_s = 1$. We observe a strong decrease in f_b when the strain direction is reversed (at 10°): BLs reform after reversal. Additionally, fewer additional links are broken in each subsequent cycle; the motion becomes less irreversible at later times. The lower 10 curves in Fig. 3(a) show f_b when the start of a later cycle is chosen as a reference frame, illustrating that the recovery of neighbors after a full shear strain cycle (at the arrow) improves with increasing cycle number.

In Fig. 3(b) we show the f_b after one cycle as a function of the starting cycle n_s, which provides a local measure of the reversibility of the configuration after one cycle. Clearly, the fraction of links broken decreases with increasing n_s

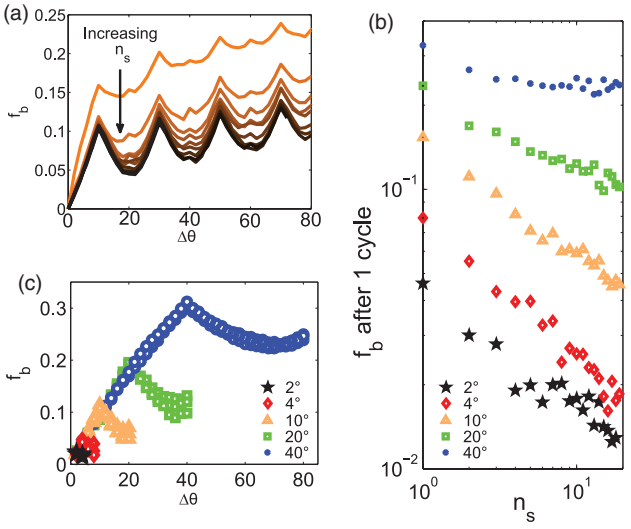

FIG. 3. (Color online) (a) Fraction of links broken, f_b, for shear reversal vs 2° strain step for the case of $\theta_r = 10°$. (b) f_b after one cycle as a function of the starting cycle n_s, for all θ_r. (c) f_b as a function of $\Delta\theta$ for representative curves at $n_s = 5$, 10 and 15.

(indicating an increase in reversibility) for all but the highest reversal amplitude, which appears to level off. As a simple local metric, f_b captures what fraction of the neighbor network is evolving with strain, a topological analog to the "particle activity" of [2]. Indeed, the apparent power dependence of the decay on n_s in the reversible regime, as well as the leveling-off for the highest reversal amplitude, is consistent with the observation of a reversible-irreversible transition observed in [2]. However, as illustrated in Fig. 3(c), f_b cannot identify this local reversibility in the neighbor network over the period of one cycle; after one cycle, f_b increases approximately linearly with cycle amplitude, without a clear change in the form of the dependence on $\Delta\theta$.

Our characterization of the irreversibility revealed a striking difference between the growth of MSDs and the fraction of links broken at driving amplitude θ_r. The MSD barely grows with θ_r for low driving amplitudes [see, in particular, Fig. 2(c) for small start cycles, where all data for θ_r from 4° to 20° strongly overlap] but then exhibits a jump for $\theta_r = 40°$. In contrast, the fraction of links broken f_b grows approximately linearly with θ_r [see Fig. 3(c)], and so, over a single strain cycle f_b fails to distinguish $\theta_r = 40$ from the lower reversal amplitudes.

We believe that this difference occurs along with the percolation of the network of links broken. In this picture, a small fraction of links broken leads to small clusters of failures that, upon reversal, are mostly healed. Consequently, after a cycle the beads return to their starting position, leading to a small MSD. However, once the fraction of links broken is sufficiently large, a dominant failing cluster forms. Upon reversal, this dominant failing cluster is not fully healed, and after one cycle, beads end up with different neighbors and at different locations, leading to a large MSD.

To probe this picture, we investigate how links that break are connected with each other by observing an aspect of the topology of the BL network. Under steady shear, it is known that the size of the largest component, i.e., the largest cluster

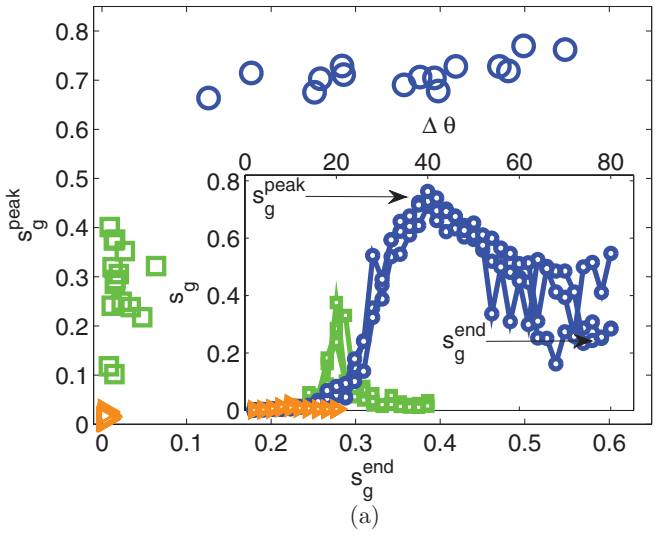

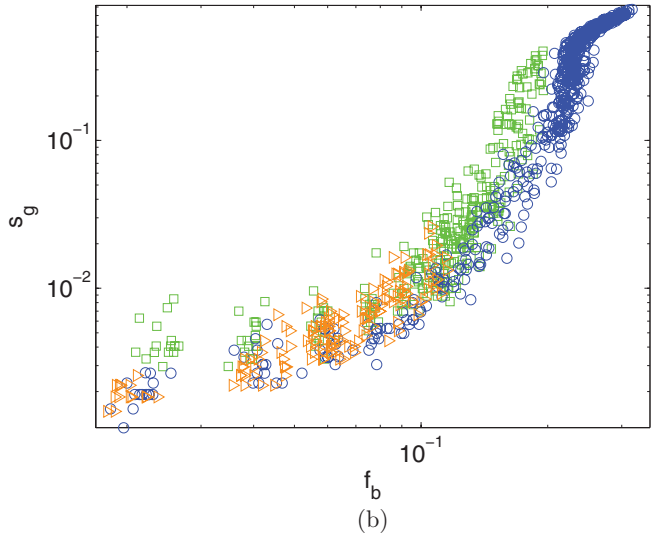

FIG. 4. (Color online) (a) The peak largest component size versus the final largest component size, for each cycle. Inset: s_g as a function of $\Delta\theta$ over one cycle for $n_s = 5$, 10, and 15. Peak and end values for s_g are pointed to for the 40° case. (b) s_g as a function of the fraction of links broken f_b for each reference network used, for θ_r of 10° [(orange) triangles], 20° [(green) squares], and 40° [(blue) circles].

of beads exhibiting inter-connected BLs, shows a transition beyond a characteristic strain (see [12]). Here we adapt this measure to oscillatory shear strain and follow s_g, which is the fraction of beads in the largest component, as a function of the absolute strain $\Delta\theta$, with reference frames chosen at the beginning of each cycle.

Figure 4 provides qualitative support for our picture. In the inset in Fig. 4(a) we show that for $\theta_r \leqslant 20°$, the size of the largest component s_g initially grows with $\Delta\theta$ but then shrinks back to almost 0 when the motion is reversed (links are reformed after reversal), while for $\theta_r = 40°$, s_g remains substantial after completing a full cycle, and hence, links remain broken. To stress this qualitative difference, we collect the data for the last 15 cycles, characterize the functional form of $s_g(\Delta\theta)$ by its peak size at the reversal, s_g^{peak}, and the largest component size at the end of the cycle, s_g^{end}, and make a scatterplot of s_g^{peak} versus s_g^{end} [Fig. 4(a)]. This reveals a clear separation of the 10° and 20° data, which form peak component sizes that can be almost fully reduced to 0, from the highest amplitude, 40°, where BLs interconnect a significant part of the system at the end of a cycle.

In Fig. 4(b) we show scatterplots of s_g versus f_b for three cycle amplitudes, which show that for each cycle amplitude, the data collapse onto a master curve quantitatively similar to that in [12]. For the highest driving amplitude, a regime emerges where s_g has a dependence on f_b that is consistent with a power law: a collective, percolation effect.

III. DISCUSSION

We have studied a granular system under shear reversal at microscopic and mesoscopic scales. Such dense systems are never found to be strictly reversible, but we have shown that irreversibility comes in two distinct flavors: spatial and topological. For low driving amplitudes, neighbor links are broken but most re-form, there are no large clusters, the MSDs are small, and, importantly, the cycle-to-cycle MSDs decrease with cycle number: the system is aging. However, for high driving amplitudes, a substantial fraction of neighbor links does not re-form upon reversal, and the cycle-to-cycle MSDs become independent of the cycle number: here the motion becomes diffusive. Our data are consistent with the hypothesis that this strong irreversibility at high cycle amplitudes is connected to the growth of a giant component, which signifies a collective breaking of contacts involving a number of beads that is proportional to the system size. We have further shown that the growth of the largest component is consistent with a power-law dependence on f_b for the highest reversal amplitude.

We note that our new topological measures of irreversibility—though less stringent than exact reversal symmetry of the equations of motion—correlate well with a strong increase in MSD with cycle amplitude [Fig. 2(c)] and, thus, are likely relevant for understanding dynamics of dense granular flows.

One important future direction of study will be to connect the onset of irreversibility in bead configuration to the emergence of dynamical heterogeneities. It is important to note that this work has probed in detail time scales much shorter than those at which dynamical heterogeneities are observed in, for instance, [7]. As a result, our observations are likely related to the formation of the building blocks of dynamical heterogeneities, whose dynamics may unfold at much larger time scales.

ACKNOWLEDGMENTS

We thank Joost Weijs for his contributions to our particle extraction routine, William Derek Updegraff for his assistance in experimentation, and Mark Hererra for his assistance in analysis. This work was supported by NSF Grant No. DMR0907146. K.R. was supported by the Rosztoczy Foundation.

[1] J. Duran, *Sands, Powders, and Grains* (Springer, New York, 2000).
[2] L. Corté, P. M. Chaikin *et al*., Nature Phys. **4**, 420 (2008).
[3] D. J. Pine, J. P. Gollub *et al*., Nature **438**, 997 (2005).
[4] M. Lundberg, K. Krishan, N. Xu, C. S. O'Hern, and M. Dennin, Phys. Rev. E **77**, 041505 (2008).
[5] O. Dauchot, G. Marty, and G. Biroli, Phys. Rev. Lett. **95**, 265701 (2005).
[6] G. Marty, O. Dauchot, and G. Biroli, Phys. Rev. Lett. **94**, 015701 (2005).
[7] R. Candelier, O. Dauchot, and G. Biroli, Phys. Rev. Lett. **102**, 088001 (2009).
[8] A. Panaitescu and A. Kudrolli, Phys. Rev. E **81**, 060301 (2010).
[9] J. Zhang, J. Ren *et al*., AIP Conf. Proc. **1145**, 553 (2009).
[10] M. Toiya, J. Stambaugh, and W. Losert, Phys. Rev. Lett. **93**, 088001 (2004).
[11] N. W. Mueggenburg, Phys. Rev. E **71**, 031301 (2005).
[12] M. Herrera, S. McCarthy, S. Slotterback, E. Cephas, W. Losert, and M. Girvan, Phys. Rev. E **83**, 061303 (2011).
[13] D. Fenistein, J. W. van de Meent, and M. van Hecke, Phys. Rev. Lett. **92**, 094301 (2004).
[14] D. Fenistein and M. van Hecke, Nature **425**, 256 (2003).
[15] S. Slotterback, M. Toiya, L. Goff, J. F. Douglas, and W. Losert, Phys. Rev. Lett. **101**, 258001 (2008).
[16] J.-C. Tsai and J. P. Gollub, Phys. Rev. E **70**, 031303 (2004).
[17] J. Crocker and D. Grier, J. Colloid Interface Sci. **179**, 298 (1996).
[18] X. Cheng, J. B. Lechman, A. Fernandez-Barbero, G. S. Grest, H. M. Jaeger, G. S. Karczmar, M. E. Mobius, and S. R. Nagel, Phys. Rev. Lett. **96**, 038001 (2006).
[19] D. Fenistein, J.-W. van de Meent, and M. van Hecke, Phys. Rev. Lett. **96**, 118001 (2006).
[20] T. Unger, J. Török, J. Kertesz, and D. E. Wolf, Phys. Rev. Lett. **92**, 214301 (2004).
[21] S. Slotterback, L. Goff *et al*., AIP Conf. Proc. **1145**, 489 (2009).
[22] J. A. Dijksman, E. Wandersman, S. Slotterback, C. R. Berardi, W. D. Updegraff, M. van Hecke, and W. Losert, Phys. Rev. E **82**, 060301 (2010).